



InGaAs/InP quantum well infrared photodetector integrated on Si substrate by Mo/Au metal-assisted wafer bonding

MIN-SU PARK, MOHSEN REZAEI, IMAN NIA, ROBERT BROWN, SIMONE BIANCONI, CHEE LEONG TAN, AND HOOMAN MOHSENI*

Bio-inspired Sensors and Optoelectronics Laboratory (BISOL), EECS, Northwestern University, 2145 Sheridan Rd, Evanston, IL 60208, USA

*hmohseni@northwestern.edu

Abstract: Integration of an InGaAs/InP quantum well infrared photodetector (QWIP) onto a Si substrate was successfully demonstrated via a metal-assisted wafer bonding (MWB) using a Mo/Au metal scheme. The Mo/Au/Mo layer, situated between the QWIP structure and the Si, has shown a well-ordered lamination. It provides a smooth surface with a roughness of about 0.8 nm, as measured by a scanning electron microscope (SEM) and atomic force microscopy (AFM). The results on crystalline quality evaluated by Raman spectroscopy and X-ray diffraction (XRD) imply that the MWB could be achieved without any measurable material degradation and residual strain. Temperature dependence of dark current revealed that there is no noticeable change in the dark current properties of the QWIP after bonding on Si, despite that the quantum wells are only 200 nm away from the bonding interface.

© 2018 Optical Society of America under the terms of the [OSA Open Access Publishing Agreement](#)

OCIS codes: (040.5160) Photodetectors; (230.5590) Quantum-well, -wire and -dot devices; (040.6040) Silicon.

References and links

1. B. F. Levine, "Quantum-well infrared photodetectors," *J. Appl. Phys.* **74**(8), R1–R81 (1993).
2. A. Rogalski, "Quantum well photoconductors in infrared detector technology," *J. Appl. Phys.* **93**(8), 4355–4391 (2003).
3. S. D. Gunapala, S. V. Bandara, J. K. Liu, C. J. Hill, S. B. Rafol, J. M. Mumolo, J. T. Trinh, M. Z. Tidrow, and P. D. LeVan, "1024 × 1024 pixel mid-wavelength and long-wavelength infrared QWIP focal plane arrays for imaging applications," *Semicond. Sci. Technol.* **20**(5), 473–480 (2005).
4. Q. Huang, G. Xu, Y. Yuan, X. Cheng, and L. Luo, "Development of indium bumping technology through AZ9260 resist electroplating," *J. Micromech. Microeng.* **20**(5), 055035 (2010).
5. J. Jiang, S. Tsao, T. O'Sullivan, M. Razeghi, and G. J. Brown, "Fabrication of indium bumps for hybrid infrared focal plane array applications," *Infrared Phys. Technol.* **45**(2), 143–151 (2004).
6. J. Wu, Q. Jiang, S. Chen, M. Tang, Y. I. Mazur, Y. Maidaniuk, M. Benamara, M. P. Semtsiv, W. T. Masselink, K. A. Sablon, G. J. Salamo, and H. Liu, "Monolithically Integrated InAs/GaAs Quantum Dot Mid-Infrared Photodetectors on Silicon Substrates," *ACS Photonics* **3**(5), 749–753 (2016).
7. S. Chen, M. Tang, Q. Jiang, J. Wu, V. G. Dorogan, M. Benamara, Y. I. Mazur, G. J. Salamo, P. Smowton, A. Seeds, and H. Liu, "InAs/GaAs Quantum-Dot Superluminescent Light-Emitting Diode Monolithically Grown on a Si substrate," *ACS Photonics* **1**(7), 638–642 (2014).
8. J. Yua, Y. Wang, J. Q. Lu, and R. J. Gutmann, "Low-temperature silicon wafer bonding based on Ti/Si solid-state amorphization," *Appl. Phys. Lett.* **89**(9), 092104 (2006).
9. R. H. Horng, S. H. Huang, D. S. Wu, and C. Y. Chiu, "AlGaInP/mirror/Si light-emitting diodes with vertical electrodes by wafer bonding," *Appl. Phys. Lett.* **82**(23), 4011–4013 (2003).
10. M. S. Park, D. M. Geum, J. H. Kyhm, J. D. Song, S. Kim, and W. J. Choi, "InGaP/GaAs heterojunction phototransistors transferred to a Si substrate by metal wafer bonding combined with epitaxial lift-off," *Opt. Express* **23**(21), 26888–26894 (2015).
11. D. M. Geum, M. S. Park, J. Y. Lim, H. D. Yang, J. D. Song, C. Z. Kim, E. Yoon, S. Kim, and W. J. Choi, "Ultra-high-throughput Production of III-V/Si Wafer for Electronic and Photonic Applications," *Sci. Rep.* **6**(1), 20610 (2016).
12. E. Higurashi, D. Chino, T. Suga, and R. Sawada, "Au–Au Surface-Activated Bonding and Its Application to Optical Microsensors With 3-D Structure," *IEEE J. Sel. Top. Quantum Electron.* **15**(5), 1500–1505 (2009).
13. E. Jing, B. Xiong, and Y. Wang, "Low-temperature Au–Si wafer bonding," *J. Micromech. Microeng.* **20**(9), 095014 (2010).

14. A. G. Baca, F. Renb, J.C. Zolper, R.D. Briggs and S.J. Pearton, "A survey of ohmic contacts to III-V compound semiconductors," *Thin Solid Films* **308–309**, 599–606 (1997).
15. A. K. Baraskar, M. A. Wistey, V. Jain, U. Singiseti, G. Burek, B. J. Thibeault, Y. J. Lee, A. C. Gossard, and M. J. W. Rodwell, "Ultralow resistance, nonalloyed Ohmic contacts to n-InGaAs," *J. Vac. Sci. Technol. B* **27**(4), 2036–2039 (2009).
16. G. Liu, G. J. Zhang, F. Jiang, X. D. Ding, Y. J. Sun, J. Sun, and E. Ma, "Nanostructured high-strength molybdenum alloys with unprecedented tensile ductility," *Nat. Mater.* **12**(4), 344–350 (2013).
17. P. Fay, K. Stevens, J. Elliot, and N. Pan, "Performance Dependence of InGaP/InGaAs/GaAs pHEMT's on Gate Metallization," *IEEE Electron Device Lett.* **20**(11), 554–556 (1999).
18. Y. Kitaura, T. Hashimoto, T. Inoue, K. Ishida, N. Uchitomi, and R. Nii, "Long-term reliability of Pt and Mo diffusion barriers in Ti-Pt-Au and Ti-Mo-Au metallization systems for GaAs digital integrated circuits," *J. Vac. Sci. Technol.* **12**(5), 2985–2991 (1994).
19. A. Gupta, D. Paramanik, S. Varma, and C. Jacob, "CVD growth and characterization of 3C-SiC thin films," *Bull. Mater. Sci.* **27**(5), 445–451 (2004).
20. M. S. Park, V. Jain, E. H. Lee, S. H. Kim, H. Pettersson, Q. Wang, J. D. Song, and W. J. Choi, "InAs/GaAs p-i-p quantum dots-in-a-well infrared photodetectors operating beyond 200 K," *Electron. Lett.* **50**(23), 1731–1733 (2014).
21. E. Altin, M. Hostut, and Y. Ergun, "Barrier lowering effect and dark current characteristics in asymmetric GaAs/AlGaAs multi quantum well structure," *Appl. Phys., A Mater. Sci. Process.* **105**(4), 833–839 (2011).

1. Introduction

Compound semiconductor based quantum well infrared photodetectors (QWIPs) have been showing a tremendous progress for infrared (IR) applications such as high resolution IR imaging from space, medical diagnosis, monitoring environment, and surveillance [1–3]. Since technology for growth and fabrication of this material system have been developed continually, large format arrays having a high pixel uniformity and operability can be mass produced [3]. Such focal plane arrays (FPAs) are typically connected to Si-based readout integrated circuits (ROICs) through indium bump and flip-chip bonding process, so that the hybrid integrated chip provides an integrated IR imaging sensor. However, indium bumping technology has limitation of high-throughput due to the tedious processes, and the fact that it is a die-level process. Although the indium bumps on the both sides are interconnected by flip-chip bonding, the unintentionally formed indium oxide on the surface of the bumps induces to decrease shear strength of the interconnection [4], and displacement of the indium bump by thermal cycle between liquid nitrogen and room temperature is incurred [5]. Furthermore, it is hard to implement the wafer-scale integration, which is the main bottleneck in mass-production of the non-silicon integrated IR imaging sensors.

In order to circumvent such integration issues, two principal different paths been considered. One approach is monolithic growth of compound semiconductor on Si platform (ROICs), using molecular beam epitaxy (MBE) or metalorganic chemical vapor deposition (MOCVD). They have an advantage of CMOS-compatible fabrication, and hence large format size and cost effectiveness. Only recently has it become possible to realize the competitive device performance by achieving a good quality of buffer layers on Si [6, 7]. However, the intrinsic threading dislocation density of the device films, which originated from the lattice mismatch and thermal expansion coefficient difference from Si, is still an impediment to their practical use and commercialization. Besides, the high temperature process to remove the native oxide or contaminants in the growth chamber is virtually impossible to be applied to fully processed ROICs [6]. On the other hand, metal-assisted wafer bonding (MWB) has been used. It effectively utilizes an intermediate thin metal to bond each other wafers. Gold–Gold (Au–Au) bonding has been extensively studied to implement the integration of compound semiconductor based device on the Si platform by taking advantage of a low-temperature process that prevents residual stress responsible for bowing or cracks [8–11]. Moreover, shear strength of Au–Au bonding has been as high as ~20 MPa [12, 13], promising a strong interconnection between the FPA and ROIC for applications in harsh environments. However, this method suffers from a propensity for deep spiking, poor controllability, and insufficient thermal stability over 300°C [14]. In order to avoid the unfavorable diffusion of Au atoms, a good diffusion barrier prior to Au deposition

is highly desired. Platinum (Pt) has been typically utilized as the diffusion barrier, thanks to its excellent resistance to corrosive acids, high temperature durability, and good ohmic contact to n-type InGaAs layers. As a result, Pt/Au double layer has been successfully achieved as the intermediate metal layer for MWB of III-V based electronic and optoelectronic devices on Si [9–11].

In this study, we have introduced molybdenum (Mo) as the diffusion barrier of MWB and evaluated the feasibility of Mo/Au bonding layer for InGaAs/InP QWIP integrated on a Si substrate. The QWIP active layer was extremely close to the bonding interface (~ 200 nm), which significantly adds to the sensitivity to any damage produced by the bonding. Mo is superior to Pt in terms of its thermal properties and the contact resistance for n-InGaAs. A metal film used for MWB with higher thermal conductivity (TC) and lower coefficient of thermal expansion (CTE) causes less cracking and deformation in transferred III-V detectors into Si substrate (ROIC). TC and CTE for Mo are 139 W/mK and 5.1×10^{-6} /K, respectively. However, Pt has a lower TC of 72 W/mK and a higher CTE of 9.1×10^{-6} /K. Besides, ultralow contact resistivity of $(1.1 \pm 0.6) \times 10^{-8} \Omega \text{ cm}^2$ from the Mo/n-InGaAs interface for application of transistors operating terahertz frequencies was reported in [15]. Therefore, Mo/Au metal scheme is more favorable for application to abrupt temperature change, high-temperature fabrication, and high-speed [15–18]. The quality of the bonded device film on the Si has been evaluated using scanning electron microscopy (SEM), atomic force microscopy (AFM), x-ray diffraction (XRD), and Raman spectroscopy. In addition, the dark current characteristics of the InGaAs/InP QWIP devices, before and after bonding to Si substrate, have been compared.

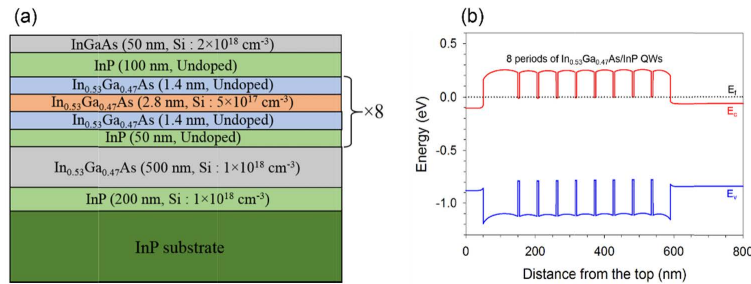


Fig. 1. (a) The epitaxial layers and (b) the energy band diagram of the as-grown QWIP at thermal equilibrium.

2. Experiment

The QWIP structure was grown by metal-organic chemical vapor deposition (MOCVD) on a (001) semi-insulating InP substrate as shown in Fig. 1(a). The epitaxial layers, from the bottom to the top, consist of a 200-nm-thick InP buffer layer, a 500-nm-thick Si-doped $\text{In}_{0.53}\text{Ga}_{0.47}\text{As}$, 8-periods of a 5.6-nm-thick $\text{In}_{0.53}\text{Ga}_{0.47}\text{As}$ quantum wells (QWs) surrounded by a 30-nm-thick undoped InP barrier, an 100-nm-thick undoped InP, and a 50-nm-thick Si-doped $\text{In}_{0.53}\text{Ga}_{0.47}\text{As}$. A 2.8-nm-thick middle layer of the QWs contains an n-type modulation doped $\text{In}_{0.53}\text{Ga}_{0.47}\text{As}$. The calculated energy band diagram shown in Fig. 1(b) displays the conventional asymmetric n-i-n QWIP structure detecting long wavelength infrared. Figure 2(a) shows the process flow of the QWIP bonding on Si substrate using the MWB technique. The process started by a solvent cleaning to remove organics on the surface of the QWIP sample and Si substrate, it followed treating the sample with NH_4OH and $(\text{NH}_4)_2\text{S}$ sequentially. The Mo/Au (10/10 nm) bilayer is deposited on both samples using an electron-beam evaporator. The two samples are then bonded to each other after surface activation with Ar-based plasma treatment. The MWB is conducted at 200°C and a uniaxial pressure of around 2 MPa for 1 hour. Then, the bonded sample was immersed in HCl (37%) to remove

the InP substrate. After removing the substrate, the AFM image displays that the root mean square (RMS) value of the surface roughness of the bonded film is about 0.8 nm as shown in Fig. 2(b). Since the surface roughness plays an important role in achieving intimate contact at the interfaces, the measured surface roughness signifies that the Mo/Au based MWB could be attained without significant contamination and the void formation.

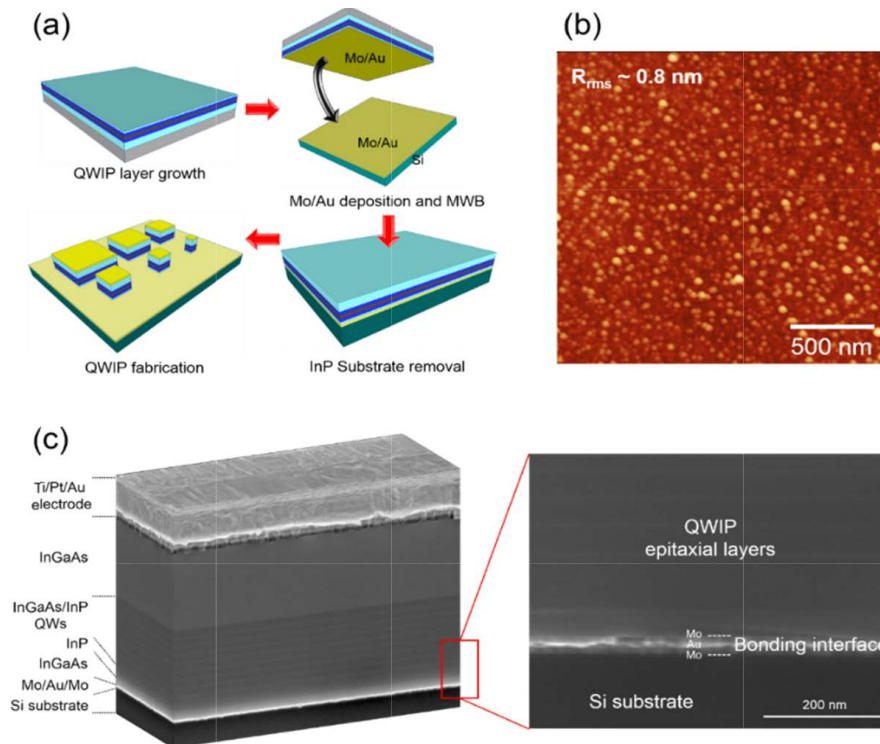


Fig. 2. (a) Fabrication process flow of the InP/InGaAs QWIP on Si wafer by Mo/Au double layer based metal wafer bonding technology. (b) AFM image of the surface of the device film transferred to Si after the removal of the InP substrate. The AFM was operated in contact mode and the scan area is $2 \times 2 \mu\text{m}^2$. (c) Schematic illustration of the fabricated device with cross-sectional SEM images and the enlarged SEM image of the bonding interface.

The device fabrication was performed using conventional photolithography and wet etching methods. For comparison of the electrical characteristics of the control device, the fabrication of the bonded and control devices was performed simultaneously. The $\text{H}_3\text{PO}_4:\text{H}_2\text{O}_2:\text{DI}$ and $\text{H}_3\text{PO}_4:\text{HCl}$ etchants were used for removing the InGaAs and InP, respectively. After the mesa formation, non-alloyed Ti/Pt/Au metallization was evaporated and lifted-off for the top contact of the bonded film. On the other hand, the metallization was utilized at the top and bottom electrodes for the control device. Figure 2(c) illustrates cross-sectional scanning electron microscopy images of the bonded device after cleaving. A reverse 8-periods InGaAs/InP MQW is clearly observed and a bonding interface of Mo/Au/Mo is well arranged between the device structure and Si. The fabricated devices were mounted in a liquid nitrogen cooled cryostat equipped with in situ electrical probes. Device dark current was measured by a multimeter (34410A) connected to a low-noise current preamplifier (SR 570) at different temperatures. The temperature of the cold shield around the devices was kept the same as that of the sensor controller (LakeShore).

3. Results and discussion

Since the strain in the crystal affects the frequency of the phonons, the strain in bonded epitaxial layers and the as-grown layers were evaluated using Raman spectroscopy. Figure 3(a) shows the Raman spectra of the samples before and after the MWB. The Raman spectra were measured in the backscattering configuration at room temperature using a $50\times$ objective lens with a 532-nm laser. The peaks of InAs-like and GaAs-like LO mode was observed in the both samples. However, the as-grown sample displays the InP LO phonon because the penetration depth of the excitation wavelength reaches as deep as the 100-nm-thickness InP layer of the as-grown sample. The bonded sample shows almost same Raman shift compared with the as-grown sample without any peak shift, indicating there is no perceptible strain in the bonded films. The films were subsequently characterized by using XRD, to investigate their crystalline characteristics. The XRD patterns for the both samples are as shown in Fig. 3(b). The XRD spectrum of the as-grown sample displays $\text{In}_{0.53}\text{Ga}_{0.47}\text{As}$ and InP diffraction peak located at 56.6° and 63.3° , respectively. The same sharp peaks of $\text{In}_{0.53}\text{Ga}_{0.47}\text{As}$ and InP are also obtained in the bonded sample. Besides, the peak corresponding to Si and the peak at 61.7° due to the $\text{CuK}\beta$ radiation diffracted from the Si (400) planes are observed in the bonded film [19]. These results from the Raman and XRD spectra confirm that the MWB could be achieved without any observable material degradation and residual strain inside the film.

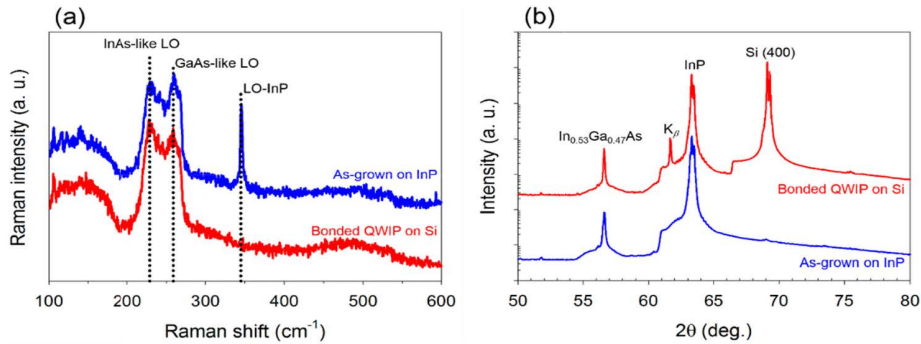


Fig. 3. Comparison of (a) Raman spectra and (b) XRD 2θ scanning between the as-grown InGaAs/InP QWIP on InP and bonded device epitaxial layers on Si.

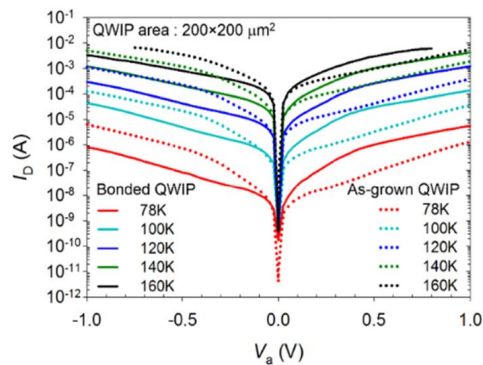


Fig. 4. Comparison of dark current versus applied bias voltage of the bonded (Solid lines) and the as-grown (Dashed line) QWIP having a $200\times 200\text{-}\mu\text{m}^2$ -area at different temperatures.

The measured dark current (I_D) of the bonded and the as-grown QWIP having a $200 \times 200 \mu\text{m}^2$ mesa area is plotted as a function of the applied bias voltage (V_a) at temperatures range from 78 to 160 K (see Fig. 4). The V_a was applied to the top electrode formed on the 50-nm-thick InGaAs for the as-grown device and on the 500-nm-thick InGaAs for the bonded device. The dark current increases with temperature due to the thermal excitation of electrons from the QWs. The I_D curves of the bonded device show mirror symmetry to those of the as-grown device around the zero bias. This symmetry is visible across the whole temperature range. For example, at $T = 78\text{K}$, the I_D of the bonded QWIP at $V_a = -0.5 \text{ V}$ and the as-grown QWIP at $V_a = 0.5 \text{ V}$ are 8.1×10^{-8} and $8.5 \times 10^{-8} \text{ A}$, respectively. There is little change in the I_D after and before the MWB, indicating that the strain resulted from thermal coefficient mismatch between the Si and the InGaAs is not likely to affect the performance of the bonded QWIP. The asymmetric I_D - V_a relationship observed in both devices is attributed to the asymmetrical $\text{In}_{0.53}\text{Ga}_{0.47}\text{As}/\text{InP}$ heterointerface [20]. When the positive V_a is applied to the electrode on the top of the thicker n-InGaAs contact layer of the devices, the higher I_D values were recorded due to the free carriers compared with those measured in the negative V_a range. We believe that the electron escape probability from the QW is larger at the thin InP barrier (50 nm) than the thicker InP barrier (100 nm) at the other side. Therefore, the electrons escaped from the QW contribute to the dark current so that the I_D of the bonded QWIP was higher in the positive bias range (Inversely, the I_D of the as-grown QWIP was higher in the negative bias range).

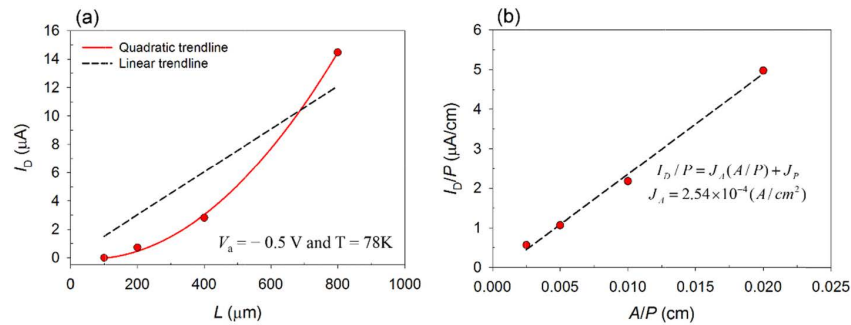


Fig. 5. (a) Dark current with respect to different side length and (b) A/P - I_D/P relationship of the bonded QWIPs at -0.5 V of the applied bias and 78K . The J_A of the device was found to be $2.54 \times 10^{-4} \text{ A}/\text{cm}^2$.

Assuming that bulk and surface are two dominant paths of the I_D for the bonded QWIP, the total dark current can be expressed as $I_D = J_A \times A + J_P \times P$, where J_A , A , J_P , and P are the bulk leakage current density, device area, the surface leakage current density, and device perimeter. Figure 5(a) shows the I_D with respect to different side length (L) of the square devices at $V_a = -0.5 \text{ V}$ and $T = 78\text{K}$. The trace of the I_D values exhibits quadratic than linear characteristics. It is found that the dominant dark current component in the bonded QWIP is bulk leakage current rather than sidewall leakage current because the I_D is proportional to the A of the devices. Since there was little change in the comparison of the I_D between the as-grown and the bonded QWIP, the I_D - L relationship of the as-grown QWIP is also likely to show a quadratic trend. The J_A taking a dominant role in the I_D can be extracted through a A/P - I_D/P relationship as shown in Fig. 5(b). The slope of the characteristic is proportional to the area-dependent leakage current so that the extracted J_A is $2.54 \times 10^{-4} \text{ A}/\text{cm}$ at $V_a = -0.5 \text{ V}$. The low dark current indicates that the active QW region in the vicinity of the bonding interface has not been damaged. Figure 6 displays the temperature dependence of the J_A for the bonded device at the different bias voltages. Linear fitting to each J_A value at the respective V_a shows good agreement. The slope of the lines can be used for the extraction of

the activation energy (E_a). The estimated E_a of the bonded QWIP is 142, 137, 129, and 117 meV at the V_a of -0.1 , -0.3 , -0.5 , and -0.7 V, respectively. The lower E_a was observed as negative bias voltage increased owing to the electric field-assisted tunneling of the carriers [21]. Since the dark current characteristics shows no significant differences between the as-grown and the bonded QWIP, the bonding quality conducted by the proposed MWB has shown great potential for integration of a wide variety of III-V based devices on silicon platforms.

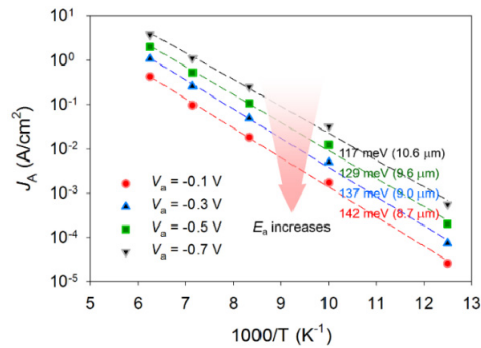


Fig. 6. Temperature dependence of the dark current density for the bonded QWIP at different bias voltages. The calculated activation energy is 142, 137, 129, and 117 meV at the bias voltage of -0.1 , -0.3 , -0.5 , and -0.7 V, respectively.

4. Summary

In summary, we established the feasibility of the Mo/Au based MWB for the InGaAs/InP QWIP integrated on silicon platforms. The bonding quality was evaluated using AFM, SEM, Raman spectroscopy, and XRD. These demonstrated that the MWB can be achieved without voids, defects, and deleterious strain. In addition, the temperature dependence of the I_D of the bonded QWIP on Si was remarkably consistent with the as-grown QWIP on InP. The bonded devices exhibited that the dark current is dominated by the bulk, the measured electronic activation energy is as predicted. Integration of QWIP within 200 nm of the bonded interface to silicon shows the robustness of the approach across a wide temperature range, making it a promising path toward image sensor integration.

Funding

Army Research Office (W911NF-16-1-0458, W911NF-11-1-0390); National Science Foundation (NSF ECCS-1542205); Materials Research Science and Engineering Center (DMR-1720139).

Acknowledgments

This work was partially supported through ARO award # W911NF-16-1-0458 and W911NF-11-1-0390. It utilized Northwestern University Micro/Nano Fabrication Facility (NUFAB), which is partially supported by Soft and Hybrid Nanotechnology Experimental (SHyNE) Resource (NSF ECCS-1542205), the Materials Research Science and Engineering Center (DMR-1720139), the State of Illinois, and Northwestern University.